Bulletin of Engineering Geology and the Environment

Seismic response of a geological, historical and architectural site: the Gerace cliff (Southern Italy)

--Manuscript Draft--

Manuscript Number:	BOEG-D-18-00882R1
Full Title:	Seismic response of a geological, historical and architectural site: the Gerace cliff (Southern Italy)
Article Type:	Original Article
Corresponding Author:	Antonio Costanzo, Ph.D. Istituto Nazionale di Geofisica e Vulcanologia Rende, ITALY
Corresponding Author Secondary Information:	
Corresponding Author's Institution:	Istituto Nazionale di Geofisica e Vulcanologia
Corresponding Author's Secondary Institution:	
First Author:	Antonio Costanzo, Ph.D.
First Author Secondary Information:	
Order of Authors:	Antonio Costanzo, Ph.D.
	Anna D'Onofrio, Ph.D.
	Francesco Silvestri, Ph.D.
Order of Authors Secondary Information:	
Funding Information:	
Abstract:	Several historical towns and sites, in Italy as well as in the rest of the Southern Europe, were edified on topographic reliefs and they host inestimable cultural heritage. In Calabria (Southern Italy), the historical town of Gerace is located in a highly seismic area and lies on the top of an unstable cliff, constituted by a soft rock slab overlying a thick clay shale formation. A comprehensive study was carried out to reproduce the seismic response of the cliff and analyze potential effects due to severe earthquakes, such as those attributed by historic documents to the Calabrian seismic sequence occurred in 1783. Many efforts were spent for the geotechnical characterisation of the soils, in particular subsoil model was obtained by combining data from field and laboratory tests. The seismic response of the cliff due to the first event of the Calabrian sequence was simulated by 1D and 2D non-linear analyses. The results permitted to assess the influence of the topography on the seismic response; also, the 2D analyses allowed to justify the occurrence of large permanent deformations, as those reported by the chronicles following the historic seismic sequence.
Response to Reviewers:	We are grateful to the anonymous reviewers and the Editor-in-Chief Prof. Louis N.Y. Wong for their constructive comments which helped us improve the quality of the manuscript. This document reports the answers ([AUT]) to the suggestions and comments. Reviewer #1: In this paper, authors introduced a subsoil model using combining data from field and laboratory tests such as Resonant Column and Cyclic Torsional Shear tests. The seismic response of the cliff due to the first event of the Calabrian sequence which was simulated by 1D and 2D non-linear analyses was detailed studied. The authors concluded that the research results permitted to assess the influence of the topography on the seismic response and the 2D analyses allowed to justify the occurrence of large permanent deformations. My comments are mainly listed as followings:

Seismic response of a geological, historical and architectural site: the Gerace cliff (Southern Italy)

Antonio Costanzo [1], Anna d'Onofrio [2] and Francesco Silvestri [2]

[1] *National Earthquake Observatory, Istituto Nazionale di Geofisica e Vulcanologia, Rende (CS), Italy, email: antonio.costanzo@ingv.it*

[2] *Department of Civil, Architectural and Environmental Engineering, University of Napoli Federico II, Naples, Italy*

ABSTRACT

Several historical towns and sites, in Italy as well as in the rest of the Southern Europe, were edified on topographic reliefs and they host inestimable cultural heritage. In Calabria (Southern Italy), the historical town of Gerace is located in a highly seismic area and lies on the top of an unstable cliff, constituted by a soft rock slab overlying a thick clay shale formation. A comprehensive study was carried out to reproduce the seismic response of the cliff and analyze potential effects due to severe earthquakes, such as those attributed by historic documents to the Calabrian seismic sequence occurred in 1783. Many efforts were spent for the geotechnical characterisation of the soils, in particular subsoil model was obtained by combining data from field and laboratory tests. The seismic response of the cliff due to the first event of the Calabrian sequence was simulated by 1D and 2D non-linear analyses. The results permitted to assess the influence of the topography on the seismic response; also, the 2D analyses allowed to justify the occurrence of large permanent deformations, as those reported by the chronicles following the historic seismic sequence.

Keywords: *Historical earthquakes; Dynamic soil properties; Numerical analyses; Seismic response; Ground deformation.*

1. INTRODUCTION

Several historical towns in Italy were edified on dominant topographic locations, mainly for strategic reasons, because this choice gave more chance to safeguard populations from the danger of barbarian attacks and invasions. However, the position of these centers did not result as much safe with respect to the natural hazards, because this particular setting often makes them highly exposed both to hydrogeological and seismic extreme events . Significant case studies showing the environmental multi-hazard of such small towns are for instance described by Fenelli et al. (1998).

As shown by comparative studies on several small centres in Italy (e.g. Lanzo et al., 2004; Costanzo et al., 2007a), the complex seismic response of cliffs, ridges and hills is affected in a different amount by topographic and stratigraphic amplification, depending on the combination of seismic input motion, geomorphological factors and geotechnical properties.

The outstanding influence of the topographic amplification on the seismic response of a homogeneous relief has been largely recognized by various analytical and numerical studies, such as those by Sanchez-Sesma (1990), Faccioli et al (2002), and Pitilakis (2004), providing a comprehensive review of topographic amplification on earthquake ground motion. In addition, different studies evaluated the seismic response of villages settled on steep morphological irregularities in order to assess the topographic effects (Paolucci, 2002; Pagliaroli et al, 2011; Massa et al., 2014).

The above studies pointed out that, for sites settled on the top of a relief, the amplification of motion results very irregular along the surface, being strongly dependent on geometrical factors, such as the predominant wavelengths of the seismic motion and the aspect ratio of the topographic irregularity. As a consequence, the topographic amplification can be often mis-predicted by means of over-simplified factors, such as those specified by most technical codes. The variability of the seismic response becomes even more complex accounting for further aspects, such as soil heterogeneity and non-linear stress-strain behaviour.

For instance, in the case of Orvieto hill (Lanzo et al., 2004) and Nicastro cliff (Pagliaroli et al., 2011), the ground response along the surface is still dominated by the coupling between the frequency content of the input motion and the topographic shape, while the stratigraphic amplification plays a minor role, being the seismic impedance poorly variable with depth. In both cases, the subsoil is constituted by soft rocks, so that non-linearity is deemed as not very significant. Another significant example is provided by the seismic response analyses of Castelnuovo hill, addressed to the seismic microzonation of this village, strongly damaged by the Abruzzo earthquake on April 2009 (Lanzo et al., 2011; Evangelista et al., 2016). Two and three-dimentional linear equivalent numerical simulations highlighted the significant dependency of the surface amplification on the elliptical shape of the relief, constituted by a thick and soft lacustrine carbonate silt deposit. Also, in this site the amplification was checked as significantly affected by the non-linear behaviour of the soft silty soil, with the linear analyses strongly overestimating the amplification factors. Additionally, the effects on the ground response due to the presence of underground cavities is also analyzed through the numerical modelling (Landolfi et al., 2014; Sica et al., 2014; Evangelista et al., 2016).

All the above examples were limited to the analyses of the transient ground motion, and did not consider the permanent ground deformation phenomena, including subsidence and slope instability, which can be triggered by strong-motion earthquakes on such sites. The seismic response of the Bisaccia hill is a paradigmatic case history in this sense: the widespread and prolonged damage of the historical centre observed after the Irpinia earthquake of November 1980 (Fenelli et al., 1992) was numerically interpreted by subsoil investigation and 2D dynamic and static analyses by Olivares and Silvestri (2001) and Lampitiello et al. (2001). The results allowed to recognize that the seismic response was affected by velocity inversion between the slab of conglomerates and the underlying clay formation more significantly than by the morphological conditions. The anomalous impedance contrast resulted into an attenuation of surface acceleration, but induced shear strain concentration in the clay: this latter factor triggered excess pore pressures slowly dissipating with time, and therefore inducing the phenomenon of long-term subsidence observed after the earthquake.

All the specific aspects characterizing the above studies, i.e. the characteristics of the earthquake input motion, the topographic and stratigraphic complexity and the non-linear soil behaviour, are shown with all their peculiar difficulties by the challenging case history presented hereafter. The following study refers to the historical centre of Gerace, located in southern Calabria, one of the most hazardous seismic region in Italy. The outstanding location of the cliff (Fig. 1) favoured the settling of different communities, since the oldest

Greek colonies to Byzantine, Arabian, Norman and Swabian dominations; all of them left evidences of historical heritage, testified by different architecture styles. Since 1939, the Italian Government imposed the landscape protection in the public interest for the natural, historical and artistic value of the centre; recently, the municipality proposed to introduce the historical centre in the UNESCO world heritage list. In such a context, this paper analyses in detail the seismic response of the cliff with reference to the first earthquake of the sequence occurred in 1783, which was accurately reconstructed in terms of reference input motions (§ 2). Some preliminary results were reported by the authors in a previous work (Costanzo et al., 2007b). The subsoil model was calibrated on the basis of the geological setting and laboratory and field investigations (§3-4); the seismic response of the cliff was simulated by 2D non-linear analyses (§ 5), in order to evaluate the transient ground motion induced by the mainshock, as well as the permanent deformation phenomena (§6).

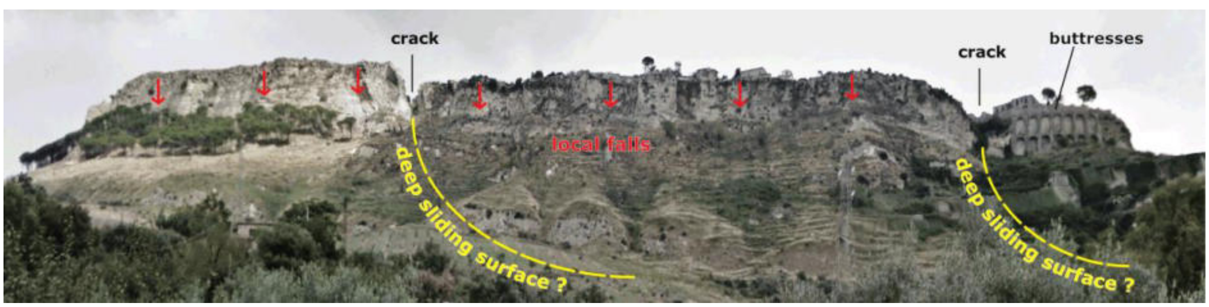

Figure 1. **Landscape view of Gerace cliff and sketch of major instability evidences.**

2. THE REFERENCE SEISMIC SCENARIO

In less than two months, i.e. since February 5 to March 28, 1783, southern Calabria was struck by five strong earthquakes, with magnitude between 5.9 and 6.9 (Fig. 2). The sequence caused the destruction of many towns (Carbone-Grio, 1887) as well as huge liquefaction and ground failure phenomena (Cotecchia et al., 1986). The environmental damage suffered at Gerace was characterised by an anomalous evolution: in fact, while the seismic epicentres shifted northwards (cf. Tab.1), the site showed repeated building damages and ground deformations, often reported as ‘landslides’ and ‘fractures’ in the Italian Strong Motion Catalogue (Boschi et al., 2000).

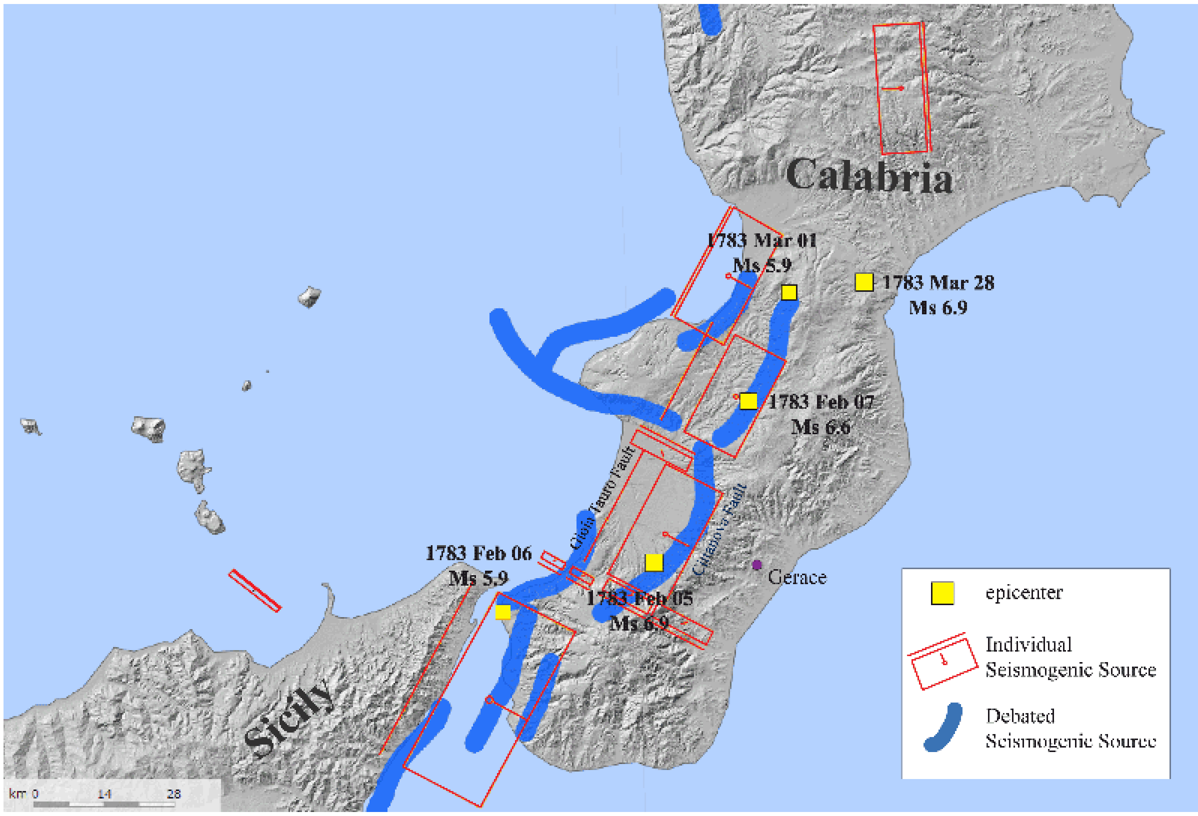

Figure 2. Seismogenic sources (modified by http://diss.rm.ingv.it/dissmap/dissmap.phtml, DISS working Group, 2018), epicenters and magnitude (Boschi et al., 2000) of the Calabrian seismic sequence in 1783.

Table 1. Magnitude of surface waves (M_S,) and site intensity (I_S) (Boschi et al., 2000), epicentral distance (d_E) and peak ground acceleration at bedrock (a_{max}) computed through hazard analyses for the town of Gerace.

Event	M_S	d_E (km)	I_S (MCS)	a_{max} (g)
1783 Feb 05	6.9	22.04	8.0	0.20
1783 Feb 06	5.9	51.76	-	0.04
1783 Feb 07	6.6	34.42	7.5	0.10
1783 Mar 01	5.9	55.95	-	0.04
1783 Mar 28	6.9	60.68	7.0	0.09

The area of southern Calabria is characterised by complex and still uncertain seismogenic sources. As a matter of fact, the distribution of macroseismic intensity and paleo-seismological studies lead to ascribe the generation of each event of the whole sequence to the different faults shown in Fig.2, evidencing an apparent interaction among them. Several assumptions were formulated in literature on the source location of the first event on February 05, 1783, attributed either to 'Cittanova Fault' (Galli & Bosi, 2002) or to 'Gioia Tauro Fault' (Peruzza et al., 1997).

Recently, some authors introduced a novel technique, based on the probability density evolution method, to take into account the randomness of the earthquakes in the seismic response analysis (Huang et al., 2015), that is the primary source of uncertainty when assessing the seismic performance of geotechnical systems (cf. Bray and Travarasau, 2007). Nevertheless, in this study a deterministic method was adopted. In fact, the authors decided to select different natural accelerograms, that could be representative of the ground motion due to the first events of the 1783 seismic sequence. Following the deterministic approach and adopting a 'macroseismic approach', the epicentre location and the magnitude were taken from Italian Parametric Strong Motion Catalogue (Rovida et al., 2016); the attenuation law by Sabetta & Pugliese (1987) was assumed, leading to estimate a peak horizontal acceleration (a_{max}) of 0.20g at Gerace. A counterproof was made following a 'seismogenic approach', the earthquake magnitude was alternatively estimated for both faults on the basis of the surface rupture length (Wells & Coppersmith, 1994); the peak reference acceleration, a_{max}, was evaluated by the attenuation law of Ambraseys (1995), by computing the distance of Joyner & Boore (1981), d_{JB}, from the fault geometry and assuming a focal depth equal to 10 km, as indicated by Seismogenic Italian Zonation (Meletti et al., 2004). Under such hypotheses, a_{max} was estimated at Gerace into the range between 0.18-0.20g both for the Cittanova fault and Gioia Tauro fault. The two approaches yielded very close evaluations of the reference motion amplitude. The macroseismic approach was extensively used also to evaluate a_{max} for all the other events (see Tab. 1), for which information about geometry of faults was either absent or incomplete (Fig. 2). Finally, the generalised attenuation relationship by Sabetta & Pugliese (1996) allowed to estimate horizontal acceleration reference response spectra for each seismic event to help for the choice of compatible accelerograms. All values of a_{max} and the response spectra are referred to the outcropping seismic bedrock.

On the basis of the above estimates, restricted ranges of magnitude and distance were fixed to select from accelerometric databases compatible records to be used as reliable input motions (Costanzo, 2007). The magnitude range of the first event (6.2<M_S<7.6) was defined assuming an overall variation of ±10% with respect to the mean estimated magnitude (M_S=6.9), with the epicentral distance, d_E, ranging between 10 and 35 km. Table 2 reports 9 different accelerometric records sorted out for the simulation of the first event. The selected accelerograms were preliminarily filtered by a Butterworth low-pass filter with a cut-off frequency of 15Hz.

Table 2. Records selected from accelerometric databases for the first event

Earthquake	Date	M_S (M_W)	d_E, d_{JB} (km)	Station	Component (° N)	a_{max} (g)	D_{rms}	F_{sc}
Landers, USA	28.VI.1992	7.5	21.0	Morongo Valley, Fire Stn 461	135	0.136	0.090	1.505
Northridge, USA	17.I.1994	7.1	*22.7*	Wonderland, California	185	0.187	0.104	1.092
Loma Prieta, USA	18.X.1989	7.1	*67.6*	Sierra Pt., San Francisco	205	0.102	0.108	1.998
Imperial Valley, USA	15.X.1979	6.9	17.5	Delta	262	0.236	0.125	0.863
El Salvador	13.II.2001	*6.6*	22.4	Col. Ext. S. Jose, San Salvador	0	0.137	0.143	1.491
Montenegro	15.IV.1979	7.0	25.0	Petrovac, Hotel Oliva	0	0.251	0.144	0.812
Duzce, Turkey	12.XI.1999	*7.1*	26.0	Duzce	90	0.276	0.145	0.738
Irpinia, Italy	23.XI.1980	6.9	32.0	Sturno	0	0.231	0.148	0.883
Chi Chi, Taiwan	20.IX.1999	7.6	*14.34*	TCU046	90	0.130	0.148	1.574

To select the most suitable real accelerograms, the approach suggested by Bommer & Acevedo (2004) was followed, computing the amplitude scale factor, F_{sc}, between the reference and the selected motion:

$$F_{sc} = \frac{a_{R\max}}{a_{S\max}} \qquad (1)$$

and the root mean square parameter, D_{rms}:

$$D_{rms} = \frac{1}{N}\sqrt{\sum_{i=1}^{N}\left(\frac{S_{a,R}(T_i)}{a_{R\max}} - \frac{S_{a,S}(T_i)}{a_{S\max}}\right)^2} \qquad (2)$$

In eqn. (2), $S_{a,R}(T_i)/a_{R\max}$ and $S_{a,S}(T_i)/a_{S\max}$ are the normalized spectral ordinates at a period T_i of the reference and selected motion, respectively; N is the number of period values used. The parameter D_{rms} supplies a quantitative evaluation of the similarity between the reference and selected spectral shape, expressing the spectral compatibility (e.g., Pagliaroli et al., 2008). Both parameters are reported in Tab. 2 for the nine selected accelerograms. The first four records in Tab. 2 are characterised by the lowest values of D_{rms}; they were therefore preferred to the others. Figure 3 shows the selected accelerograms, scaled to a_{max}=0.20g (left), and the comparison with the reference response spectra (right).

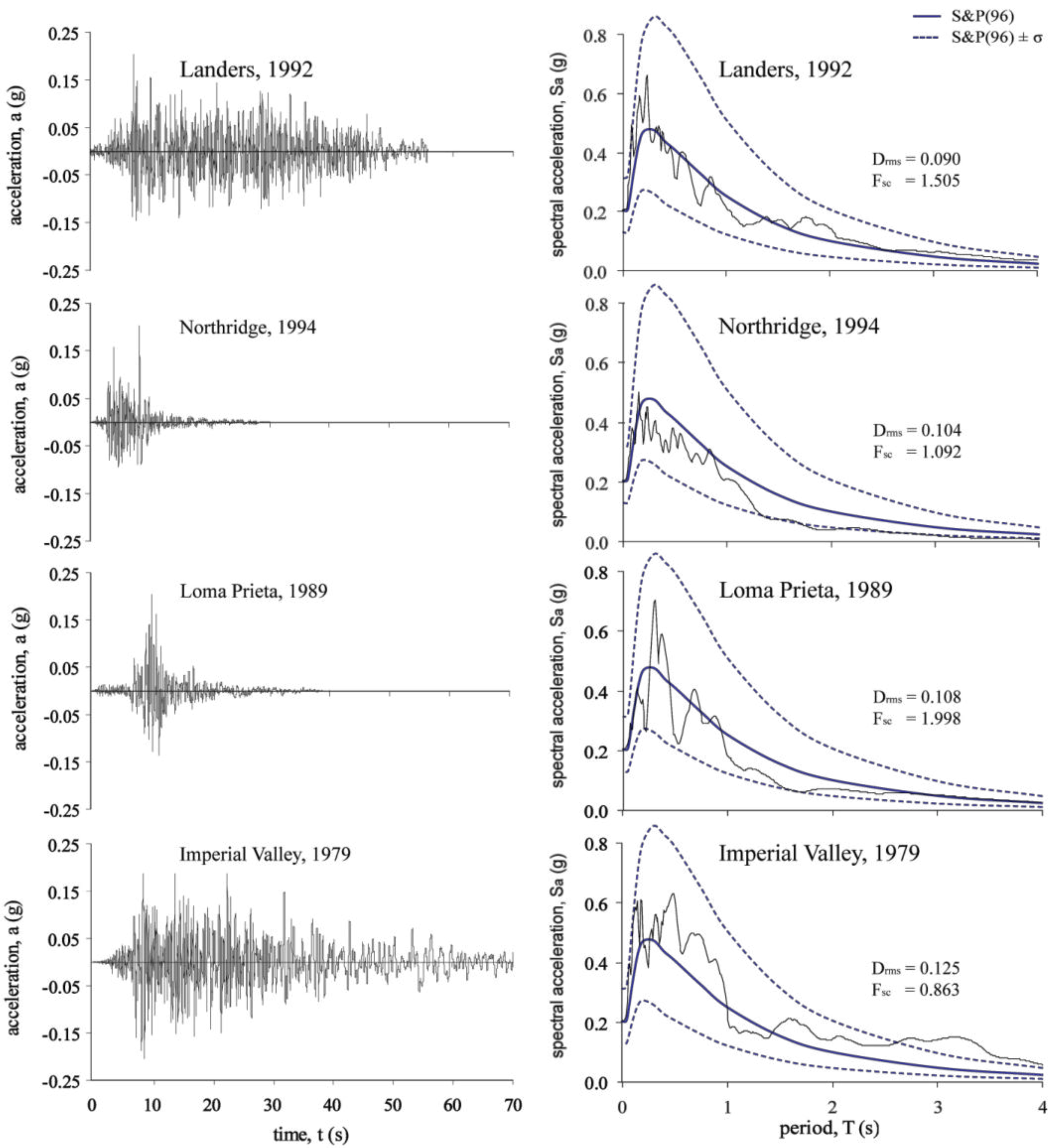

Figure 3. Selected input motions: accelerograms (left) and spectral compatibility using the relationship S&P(96) (Sabetta & Pugliese, 1996) (right).

3. GEOLOGICAL SETTING

The town of Gerace is settled at about 450m a.s.l. on a cliff oriented in NW-SE direction, between the basins of two rivers, characterised by continuous gully erosion affecting the stability of the valley borders. The cliff has been for a long time affected by slope instability problems, evidenced by cracks, falls, slides and flows. In the last years, such movements have been continuously requiring local countermeasures, as anchors and buttresses (see Fig. 1). Large scale geomorphological studies suggested that all these scattered phenomena can be viewed as shallow evidences of a deep gravitational seating, located in the clay shale formation and extending up to the superjacent soil layers (Guerricchio, 2005). Past and recent chronicles report that most of the instability phenomena have been triggered by intense rainfalls; however, there are records of repeated large deformations and landslides induced by strong earthquakes, including those occurred in 1783 (Fortunato et al., 2012).

The geological map in Fig. 4a shows the limits of the different formations, as well as the locations of previous and recent subsoil investigations.

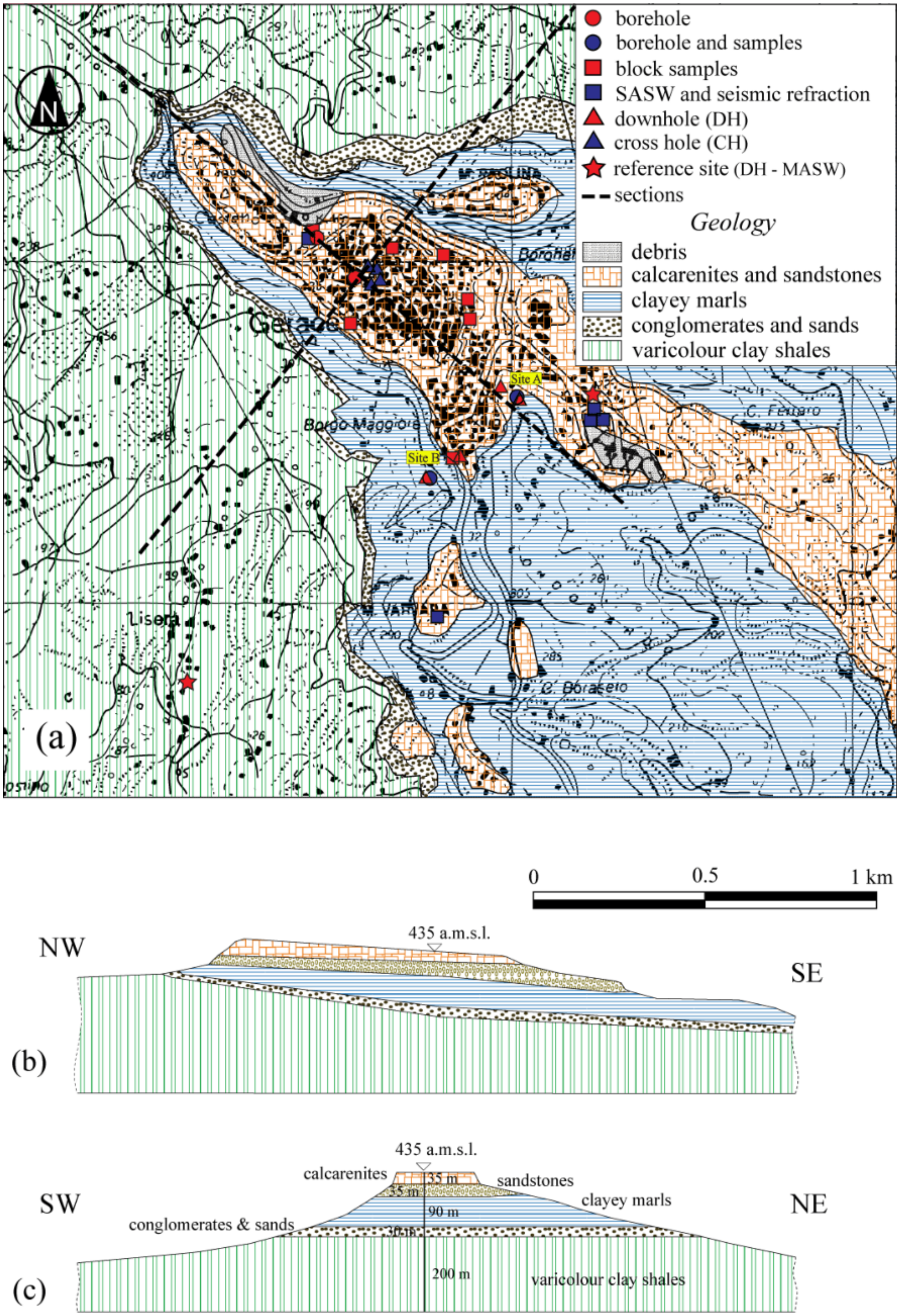

Figure 4. **Geological map with investigation sites (a) and sections NW-SE (b) and SW-NE (c).**

The upper part of the cliff is formed by a slab constituted, in sequence, by a thick layer of Pliocene calcarenites and weakly cemented sands (about 70m), overlying a deep formation of clayey marls (around 90m), which in turn rests on a relatively thinner (30m) layer of interbedded sands and conglomerates. The slab floats on a deep layer of Oligocene varicoloured clay shales, with an estimated thickness of about 200m. The current geomorphological setting is the result of the intense erosion processes, producing the progressive removal of the soils overlying the clay formation.

In 1997 several boreholes of variable depths and inclination were executed along the ridge of the cliff (white circles in Fig. 4a), for the design of stabilisation works committed by the Municipality; they allowed to take numerous calcarenite samples, subjected to unconfined compression tests in laboratory. The two deep drillings up to 200 and 120m (red circles on the calcarenite slab at the intersection of the section lines and moving towards NW along SE-NW section line, respectively) allowed to identify the complete subsoil layering, down to the varicoloured clays, and to detect the groundwater table at the top of the clayey marls. In the same period, further investigations, including Cross-Hole tests, were planned in the old town centre for the restoration of the Cathedral (blue triangles). On such a basis, the stratigraphic sections in Figs. 4b,c were sketched.

More data have been collected in 2006-2007 from a number of shallower investigations in the lower SE part of the town, carried out for the design of further stabilisation works, including down-hole profiles and laboratory tests on sands and marls (red triangles and blue circles in Fig. 4a). In the same area additional data were available from seismic refraction surveys (blue squares at SE) executed for the construction of a theatre.

The authors planned two more investigation sites, one again in the SE area, and another in the SW river valley, where varicoloured clays outcrop (red stars); surface and borehole seismic tests were executed and undisturbed samples were retrieved at different depths. Shallow samples of calcarenite and weakly cemented sand were also extracted from excavation pits along fresh slope faces (red squares).

4. GEOTECHNICAL CHARACTERISATION

The subsoil model for the seismic response analyses was obtained from the previous investigations by combining the data gathered through dynamic in situ and laboratory tests.

All the laboratory tests were carried out at University of Naples by means of a Resonant Column/Torsional Shear device (d'Onofrio et al., 1999) which allowed to characterise the non-linear cyclic behaviour of most of the soil units.

Shear wave velocity measurements on the clayey marl (Fig. 5a) were obtained by couples of Down-Hole tests located uphill (U) and downhill (D) along two steep slopes (sites A and B reported in Figure 4a), where the cliff showed instability during 2006. The profiles reported in Fig. 5a show V_S values increasing with depth down to about 10m, where the subsoil is constituted either by loose covers of sands (uphill), or by weathered marl (downhill). The downhill DH profiles appears quite scattered probably because of the different degree of weathering suffered at the two sites. By averaging the different measurements and extrapolating them to higher depths, a mean constant value of 800 m/s was assumed for the clayey marl in the geotechnical model adopted for the seismic site response analyses (Fig. 5d).

Surface wave (MASW) and Down-Hole tests were carried out by the authors in two sites, where the sand and varicoloured clay shale units outcrop (see Fig. 4a). The shear wave velocity profiles in the sand showed a good agreement among the different testing techniques (compared each other in Fig. 5b) and with the values found for the sand covering the marl formation (verticals UA and UB in Fig. 5a). The average value of V_S = 400 m/s was then attributed to the sand formation in the geotechnical model (Fig. 5d). The DH test allowed to identify the presence of a stiffer layer of calcarenite at 8-10m depth, confirmed by the stratigraphic log, but not detected by the surface wave tests. On the basis of such measurements, a V_S value of 750 m/s was assigned to the deep intact calcarenites (Fig. 5d), while a V_S = 400 m/s was assumed for the shallow fractured calcarenite, on the basis of the results of the above mentioned Cross-Hole tests carried out close to the Cathedral in 1997.

Due to the lack of previous investigations, the major experimental efforts were spent in the characterisation of the varicoloured clay shale, at the test site in the SW valley at the toe of the cliff. A first borehole was conditioned for the installation of two Casagrande piezometers, which detected the groundwater table at 10 m depth. Another borehole was cased for the execution of DH tests. Just like found in the previous test site, the different geophysical tests also provided comparable V_S profiles (Fig. 5c).

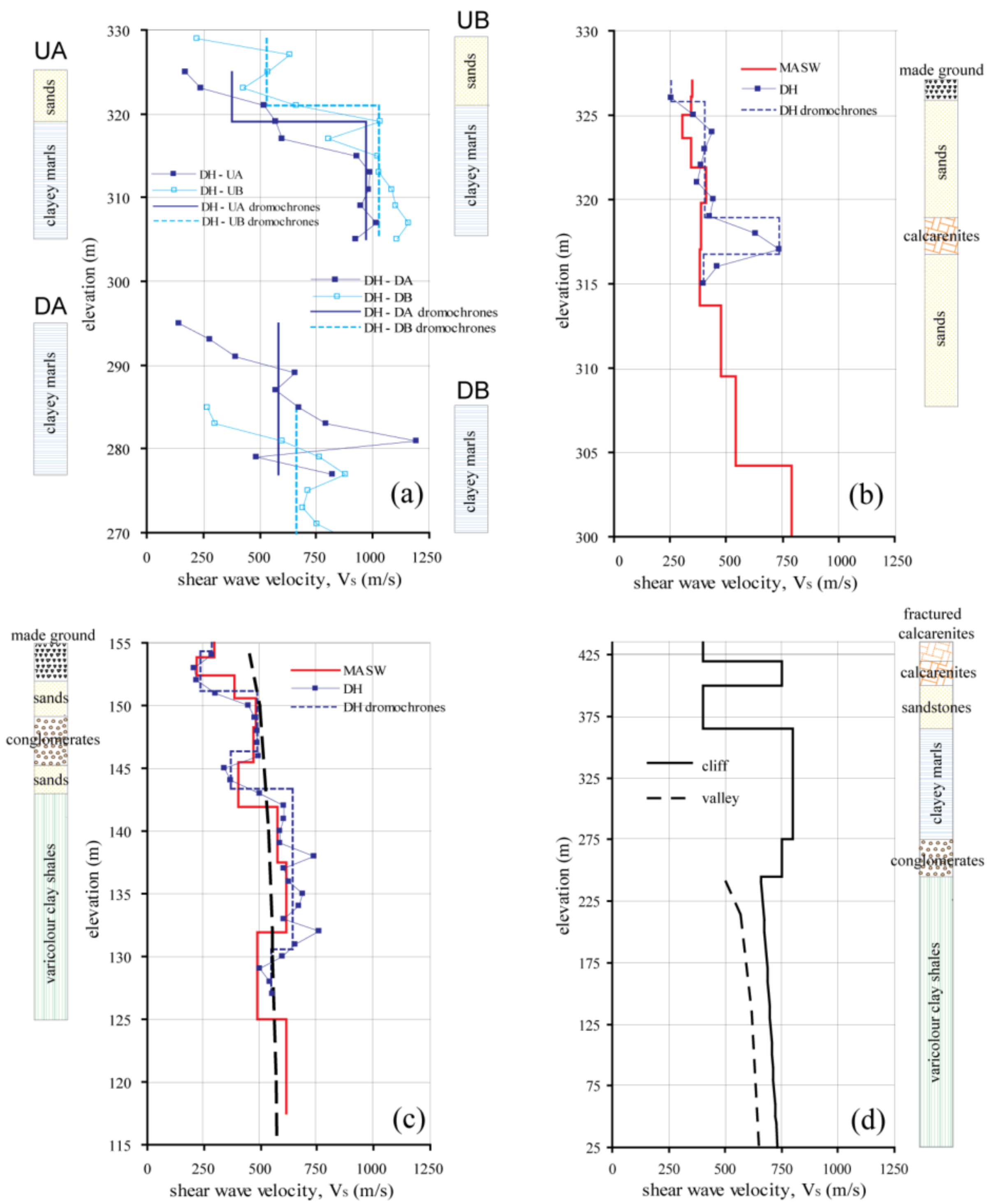

Figure 5. Shear wave velocity profiles measured at outcrops of marl (a), sand (b) and varicolour clay (c); subsoil model assumed for the seismic site response analyses (d).

Four undisturbed samples were retrieved from the same borehole, in order to carry out Resonant Column and Cyclic Torsional Shear (CTS) tests. The experimental programme was addressed to characterise the dependency of the cyclic stress-strain behaviour on the variable in situ stress state and history sustained by the varicoloured clay: namely, the overburden compression for the deposit underlying the cliff, and the swelling, due to the erosion, for that outcropping in the valley. To reproduce in the RC-CTS tests the in-situ stress paths undergone by the highly compressed clay shale, two specimens were subjected to a multi-stage consolidation sequence, starting from the estimated mean in situ stress state (≈400 kPa) and then loading up to 800 and 1200 kPa. Another specimen, instead, was left swelling under an isotropic effective stress of 200 kPa, lower than the estimated mean overburden pressure.

The G_0 values measured by RC tests carried out following the two different stress paths are plotted in Fig. 6a as a function of the mean effective stress, *p'*, and best-fitted adopting the power function reported herein (expressing G_0 MPa and *p'* in kPa):

$$G_0 = A \cdot (p')^b = 49 \cdot (p')^{0.25} \tag{3}$$

This latter is and drawn with a solid line in the same figure. The dependency of the small strain stiffness, G_0, on stress state and history was modelled distinguishing the V_S profiles under the cliff respect to that characterising the surrounding valley. Following the approach introduced by Rampello et al. (1994), the relationship between G_0, the current stress state and the stress history of the soil can be expressed as follows:

$$\frac{G_0}{p_r} = S \cdot \left(\frac{p'}{p_r}\right)^n \cdot \left(\frac{p'_y}{p'}\right)^m \tag{4}$$

In eqn. (4), the coefficient *S* represents the stiffness of the clay when normally consolidated at a reference stress state $p'=p_r$ (typically taken equal to the atmospheric pressure), the exponent *n* defines the rate of variation of G_0 with the normal consolidation stress, and *m* accounts for the dependency of G_0 on the overconsolidation ratio. With reference to a given unloading-reloading compression path, characterised by a yield stress p'_y, eqn. (4) can be re-arranged as follows:

$$G_0 = S \cdot (p_r)^{1-n} \cdot (p'_y)^m \cdot (p')^{n-m} \tag{5}$$

By comparing the power functions (3) and (5), it can be observed that

$$b = n - m \Rightarrow n = b + m \tag{5a}$$

and

$$A = S \cdot (p_r)^{1-n} \cdot (p'_y)^m \Rightarrow S \cdot (p_r)^{1-n} = \frac{A}{(p'_y)^m} \quad (5b)$$

therefore, it is proportional to the yield stress.

The behaviour of the clay shale under the cliff was assumed as normally consolidated and modelled by the equation:

$$G_0 = S \cdot (p_r)^{1-n} \cdot (p')^n \quad (6)$$

It was not possible to measure shear modulus at normally consolidated states, given the maximum confining pressure (no more than 800 kPa) applicable with the available RC-TS device. For this reason some assumptions had to be made. The yield stress p'_y was assumed to be equal to the mean overburden stress acting on the clay shale lying under the cliff at the depth of the retrieved sample, estimated to be about 2.88 MPa; the exponent m was taken equal to 0.35, by averaging literature data relevant to natural clays of Southern Italy with comparable plasticity and macro-structure (d'Onofrio et al., 1998). Taking account for the values previously found for A and b and those assumed for p'_y and m, using the equations (5a) and (5b) the following power law was obtained to describe the G_0 dependency on stress state, in normally consolidated conditions :

$$G_0 = 3 \cdot (p')^{0.6} \quad (6a)$$

The relationship is plotted in Fig. 6 with a dashed line.

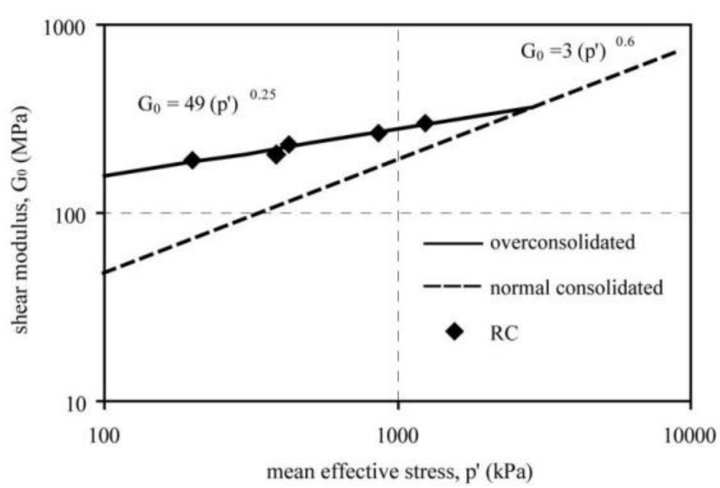

Figure 6. Dependency of the initial shear modulus on the stress state and history for the varicolour clay

The above eqns. (5) and (6) were then expressed in terms of V_S:z relationships, and scaled to the V_S values measured in situ (not affected by sampling disturbance and reconsolidation techniques). As a result, the shear wave velocity profiles drawn in Fig. 5c-d was obtained, showing that the velocity values in the valley (450-650 m/s), due to the swelling of the varicoloured clay, are consistently lower than those underneath the slab (660-725 m/s).

The laboratory tests on clayey marls and varicoloured clays also allowed to describe the non-linear behaviour of these fine-grained soils. The variation of the normalised shear modulus, G/G_0 (Fig. 7a-b), and damping ratio, D (Fig. 7c-d) with shear strain, γ, were assumed on the basis of CTS tests driven at the frequency closest to the dominant range of the earthquake motions. The characterization of the varicoloured clay lying under the cliff and in the valley was obtained from the laboratory data respectively pertaining to the compression and swelling loading paths (Fig. 7b-d), with these latter corresponding to a higher degree of non-linearity and higher damping values. The non-linear behaviour of the soils was best-fitted through the hyperbolic stress-strain model and the Masing criteria (Hardin & Drnevich, 1972), to be effectively used in the numerical SSR analyses. The same graphs also show the curves for the sands (Fig. 7a-c) and conglomerates (Fig. 7b-d), as derived from literature indications relevant to soils with comparable lithology, respectively given by Lo Presti et al. (1997) and Marcellini et al. (1995).

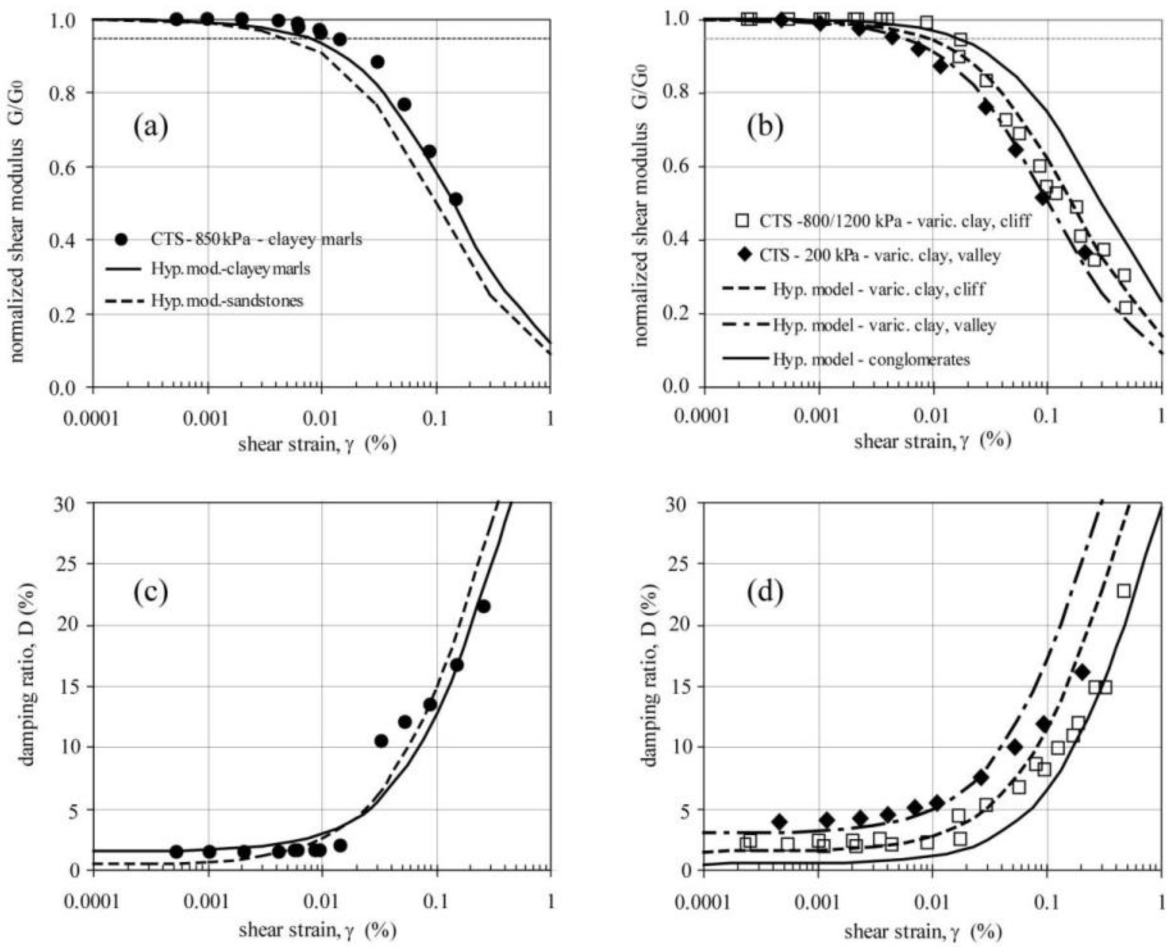

Figure 7. **Strain-dependent equivalent parameters for sand and marl (a,c), conglomerate and varicolour clay (b,d).**

The calcarenite was assumed as a linear material, as well as the bedrock, which was assumed to be a stiff rock elastic half-space, underlying the clay layer at a depth of about 200m, as indicated by previous geological studies (Monteleone, 1993) and, indirectly, verified through comparison between experimental and numerical frequency content, in the latter case by varying the thickness of the varicoloured clay layer (Costanzo, 2007).

Table 4 shows a summary of the parameters used for the numerical simulations described in the following section. The shear wave velocity V_S is set constant for all formations, except for the varicoloured clay shales, where it varies with depth. The measurements of the compression wave velocity, V_P, in the Down-Hole tests allowed to set the values of the Poisson's coefficient, ν, for all soils. The shear and compression moduli were obtained on the basis of V_S and V_P, and of the average unit weight, γ, measured on undisturbed samples. The small strain damping, D_0, was taken from CTS test results, when available, or from the literature in the other cases.

Table 4 also contains the volumetric threshold strain (γ_v), corresponding to the value for which shear-volumetric coupling (i.e. volume changes or pore water pressure build-up) is expected to be triggered. Since no reliable measurement of pore pressure build up were obtained from the RC and CTS tests, the volumetric threshold, γ_v was assumed as corresponding to the strain level for which G=0.65G_0, as suggested by Vucetic (1994). The effective strength parameters, c′ and φ′, of the sand and fine-grained soils were obtained from direct shear tests on undisturbed samples, while those of the calcarenite were derived from uniaxial compression tests (Costanzo, 2007). The strength parameters of the conglomerate were attributed on the basis of the above mentioned literature indications on similar soft rocks.

Table 4. Soil parameters for seismic site response analyses.

Material	γ (kN/m^3)	V_S (m/s)	V_P (m/s)	ν	D_0 (%)	γ_v (%)	φ' (°)	c' (kPa)
Fractured calcarenite	16.69	400	693	0.250	0.5	Linear	35	7
Calcarenite	16.69	750	1299	0.250	0.5	Linear	40	700
Sandstone	16.94	400	781	0.322	0.5	0.048	35	54
Clayey marl	18.05	800	1595	0.332	1.5	0.060	32	34
Conglomerate	19.51	750	1368	0.285	0.5	0.160	30	1000
Varicoloured clay (cliff)	21.00	658 725	1612 1776	0.400	1.5	0.068	25	0
Varicoloured clay (valley)	20.87	454 643	973 1379	0.361	3.0	0.040	25	0
Bedrock	22.00	1500	2806	0.300	0	Linear		

5. NUMERICAL MODELLING OF THE SEISMIC RESPONSE

The seismic response of the cliff and the surrounding valley was simulated by one-dimensional and two-dimensional analyses with different numerical methods.

One-dimensional analyses were executed with the conventional linear-equivalent approach using the well-known EERA code (Bardet et al., 2000). Two-dimensional non-linear analyses were also carried out adopting the finite difference code FLAC 5.0 (Itasca, 2005), aiming to investigate both the influence of the complex 2D topography on the seismic ground motion at surface and the permanent deformations extent developed along the cliff profile. In the 2D analyses, the pre-failure soil behaviour was assumed as characterised by the same parameters adopted for the 1D analyses (see Tab. 4 and Figs. 5d-6-7), with the hysteretic damping modelled applying the Masing criteria to the shear modulus decay curves fitted by the hyperbolic model. The small-strain viscous damping was included in the FDM algorithm according to the well-known Rayleigh formulation, i.e. assuming that the damping tensor [C] is a linear combination of the mass [M] and the stiffness [K] tensors:

$$[C] = \alpha[M] + \beta[K] \tag{7}$$

For each soil layer, coefficients α and β were chosen according to the values of the small-strain damping ratio, D_0, reported in Tab. 4. A double frequency approach (Hashash & Park, 2002), was calibrated to yield the same damping-frequency function as the single frequency method used by the program (Costanzo, 2007). Soil behaviour at failure was represented by a Mohr-Coulomb plastic envelope, with a non-associated flow rule.

Figure 8 shows the mesh grids used to model the two geological sections of Fig. 4, which represent also the actual topographic aspect of the cliff. It is worth mentioning that the models do not take into account any differences respect to the topographic setting at the time of the historic earthquakes. Nevertheless, although some local morphological changes may have occurred in about 200 years, the topographic aspect seems enough similar to that reproduced in an engraving sketched about 80 years before the seismic sequence, and however small changes are virtually impossible to reconstruct with due reliability.

The thickness of the mesh elements was set between 5m and 10m throughout the whole grid. According to the well-known rule of the thumb by Kuhlemeyer & Lysmer (1973), these sizes correspond to a maximum frequency of about 10 Hz propagated in the subsoil profile (e.g., for the softest soil V_S=400 m/s with thickness of 5m, cf. Fig. 5 and Table 4). The seismic input motions, sampled at 0.01 s, were preliminarily low-pass filtered to a frequency of 15 Hz, and the time step in the integration was set equal to $5 \cdot 10^{-5}$ s. Preliminary calibration tests (Costanzo, 2007) demonstrated that the choice of a finer mesh size and of a narrower low-pass filtering did not significantly improve the computed response.

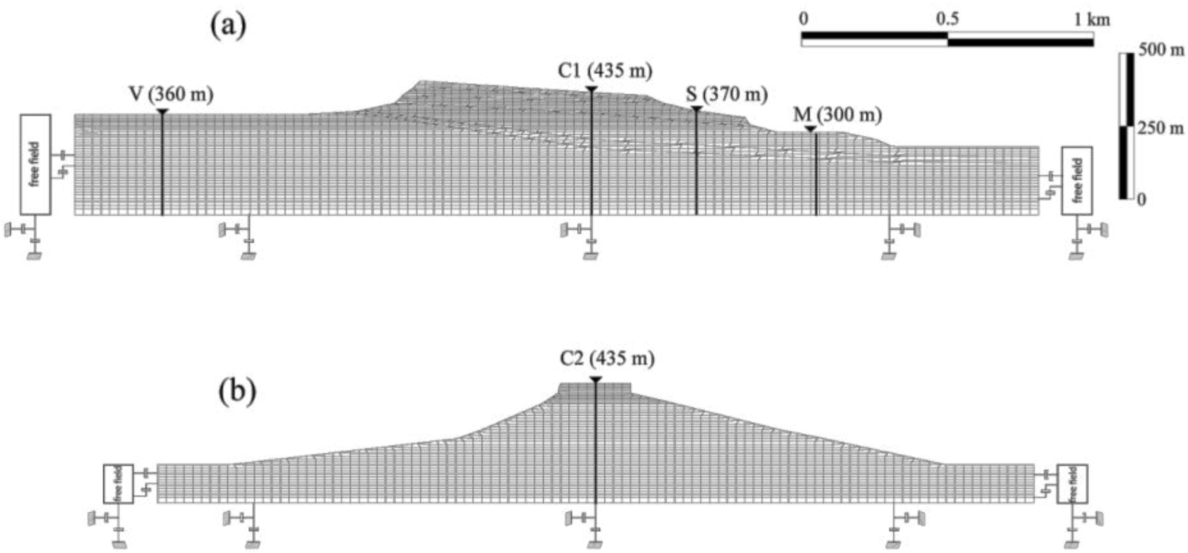

Figure 8. **Meshes for FDM analyses: NW-SE (a) and SW-NE (b)**

To avoid undesired wave reflections in correspondence of the domain borders, a 'quiet boundary' condition was adopted for the bedrock, consisting of viscous dampers acting along normal and tangential directions (Lysmer & Kuhlemeyer, 1969). In addition, the mesh was extended for at least 250 m on each side of the hill, and 'free-field boundary' conditions were used at the lateral borders. These latter consist of one-dimensional columns simulating the behaviour of a lateral semi-infinite medium, linked to the mesh grid through viscous dashpots (Itasca, 2005).

6. SEISMIC AMPLIFICATION AND PERMANENT DISPLACEMENTS

The seismic response to the first earthquake of the sequence, simulated using Landers earthquake – which showed the better compatibility with the reference spectrum (cf. Table 2) –, is plotted in Fig. 9 in terms of vertical profiles of peak acceleration (plots a-d), shear strain (plots b-e) and stress (plots c-f). The upper plots show the response computed by 1D (dashed line) and 2D analyses (C1, C2 data sets) along the vertical central axis of the calcarenite slab, where the two sections intersect (Figs. 4-8). The lower plots report the 2D response at different sites, located along the NW-SE section, at the outcrop of sandstones (S), marls (M) and varicoloured clays (V).

At the hill centre, the peak acceleration profile (full squares in Fig. 9a) obtained from the 2D analysis along the NW-SE longitudinal section is in a good agreement with the 1D response; instead, higher acceleration values were calculated along the same vertical axis, considering the SW-NE transversal section (full triangles). Most of the amplification is concentrated along the uppermost 100m, in particular at the contact between intact and fractured calcarenites and, mostly, between marls and sandstones. Similar amplification phenomena are evident also along the S vertical, in the outcropping sandstone formation (Fig. 9d). The localization of the amplification along the vertical profiles is therefore mainly due to the high impedance contrast between marl and sandstone. A significant amplification is also evident in the upper part of M profile, whereas along the outcropping clay vertical (V) the acceleration at surface results slightly lower than at the bedrock (Fig. 9d).

The sandstone formation also exhibits the maximum peak shear strain values. Along both sections (see C1, C2 and S profiles in Fig. 9b,e), γ_{max} systematically exceeds the volumetric threshold γ_v, which is of the order of 0.05% for this material (see Table 4), inducing to expect permanent volumetric and shear strains. The 1D and 2D shear stress profiles along the central axis of the cliff (Fig. 9c) show similar trend, even if the latter are characterized by greater variability with depth, particularly along the NW-SW section (C2 profile) where a relative maximum at the contact between sandstones and clayey marls is clearly detectable.

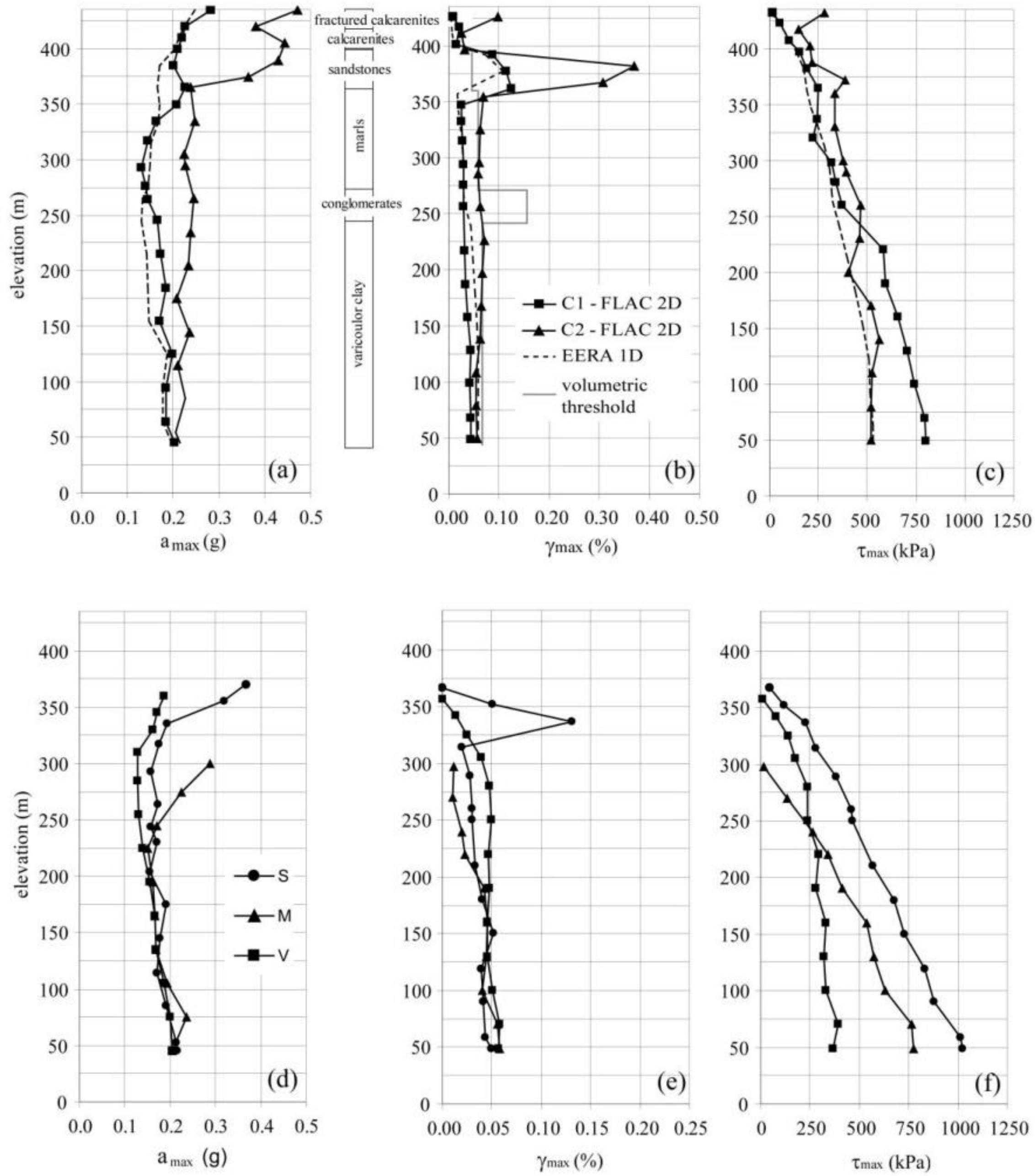

Figure 9. Vertical profiles of peak acceleration (a,d), shear stress (b,e) and strain (c,f) at different sites.

The response spectra in Fig. 10a,b highlight the combined effects of stratigraphic and topographic amplification on the seismic response at the surface.

The spectral accelerations at different point along the longitudinal section are compared to the input motion in Fig. 10a. The varicoloured clay site (vertical V) shows a quite uniform spectral amplification throughout the entire range of periods; marls (site M) and sandstones (site S) mostly amplify at frequencies higher than 1Hz, showing a peak spectral acceleration exceeding 1g at a period of about 0.25s and 0.40s, respectively; the outcropping calcarenite layer (C1) seems to enhance the response at higher periods.

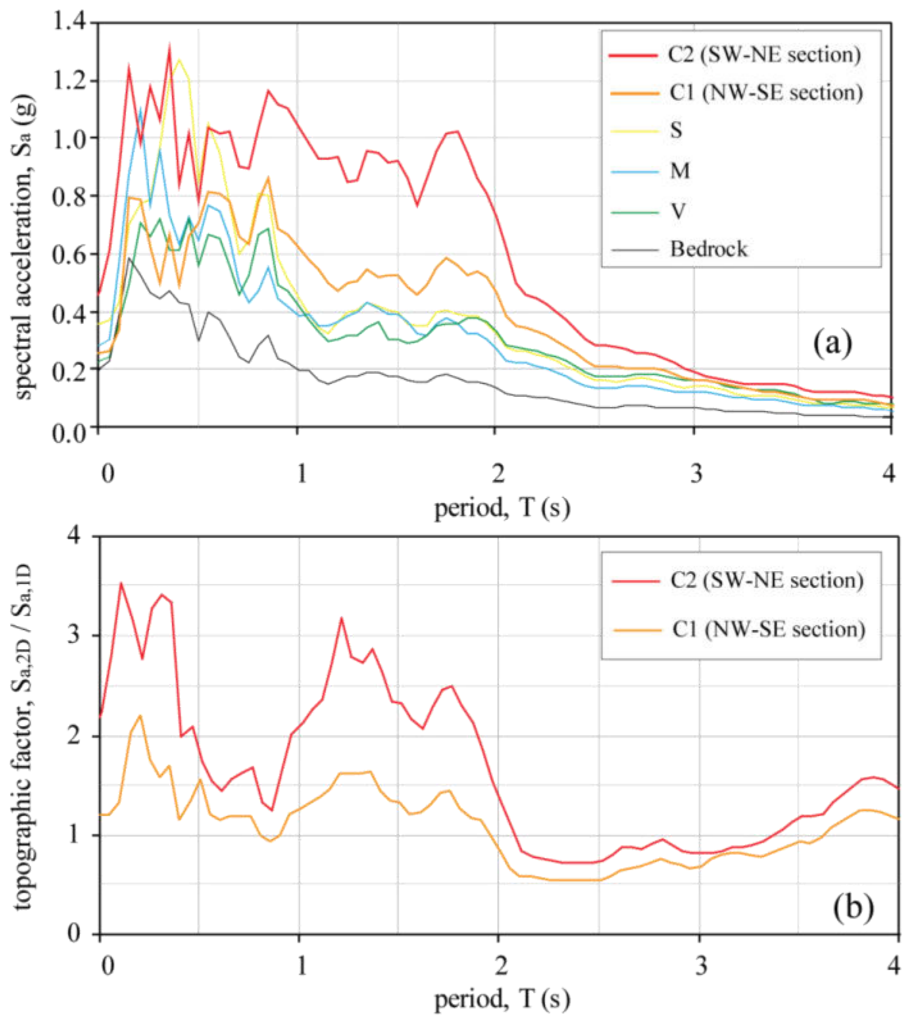

Figure 10. Response spectra showing stratigraphic amplification (a) and topographic factor (b).

In Fig. 10b, the spectral acceleration predicted at the town centre by 2D numerical analyses along both cross sections (C1 and C2 profiles) is normalised respect to that computed by 1D analysis with EERA to highlight the topographic effect. Along the NW-SE direction, where the topographic effects are expected to be less significant, the 1D and 2D response are indeed very similar, except for the low-period range where the peak spectral acceleration of the input motion is enhanced by the 2D geometry. The spectral amplitudes at the C2 profile relevant to the SW-NE section are significantly higher than those calculated along the NW-SE section, confirming that topographic amplification affects more significantly the transversal section of the hill.

The amplification factor of the peak ground acceleration is plotted in Fig. 11 a-b along the two analyzed sections, for the four different input motions showed in Fig.3. The shapes of the topographic profiles are added for comparison. The seismic response does not seems to be strongly influenced by the input motion, at least in the case of the SW-NE section, whereas a slight effect is more evident along the NW-SE section. Landers input signal give rise to the highest amplification ratios along the two sections. The alternating amplification and attenuation of the peak acceleration along the slopes of the cliff can be ascribed to the interaction between incident and diffracted waves. The response of the central part of the cliff in the NW-SE section is characterized by an average amplification factor of 1.5, which increases up to 2.5 moving towards the edges (Fig. 11a). The SW-NE section instead shows higher amplification factors at the top of the hill (Fig. 11b) due to both the resonance of the cliff and to the focalization of body waves associated to the narrow profile, that induces a more pronounced topographic effect.

In Fig. 11c the amplification factor at the C2 node (on the surface of the section SW-NE) is plotted as spectral acceleration ratio; amplification is predicted on the entire period range, whichever is the input adopted. The acceleration spectral ratio shows mean values higher than 4 between 1.0s and 1.8s, emphasising the combining of stratigraphic and topographic effects.

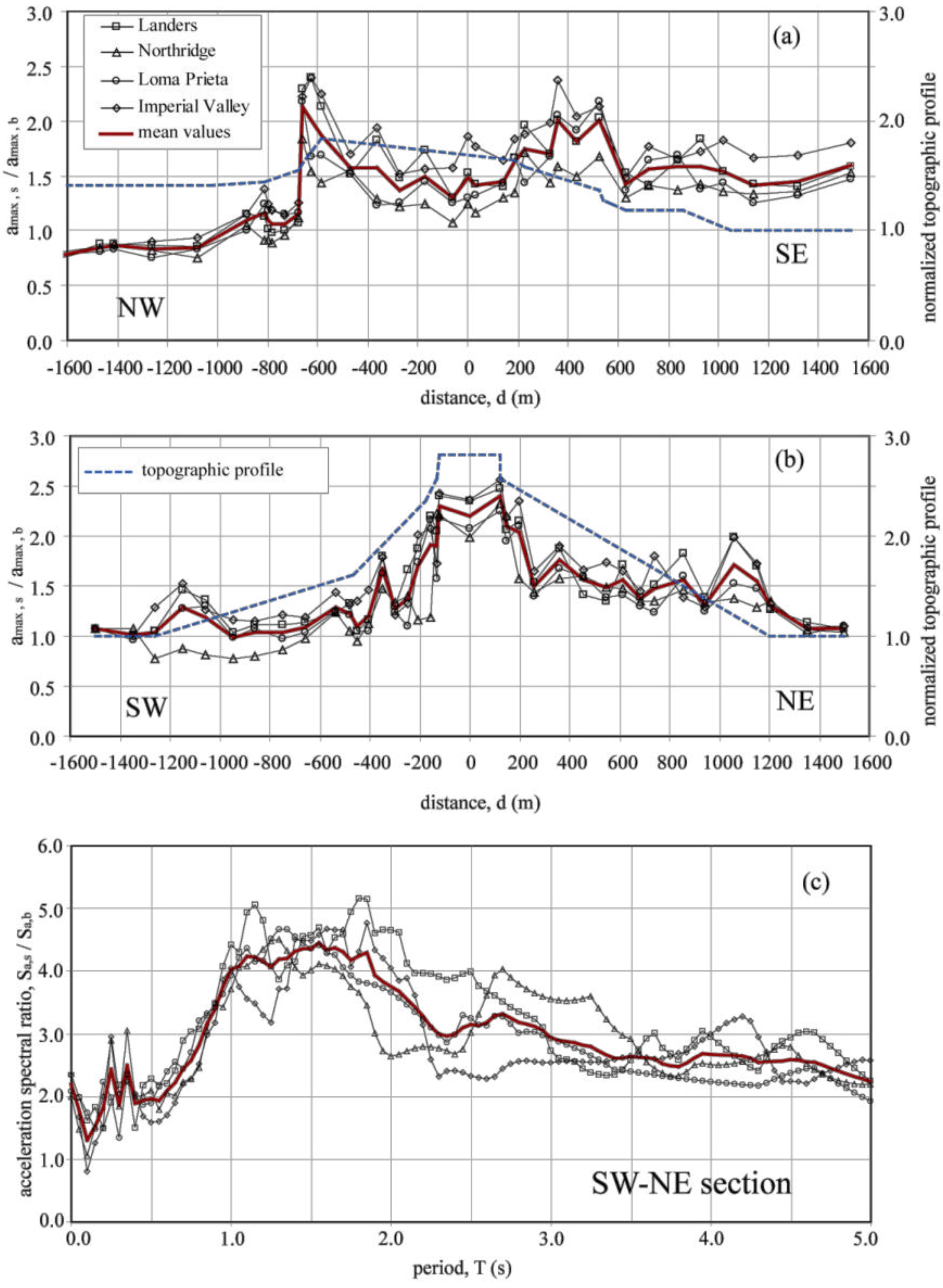

Figure 11. Amplification versus topographic profiles along NW-SE (a) and SW-NE (b) sections, and acceleration spectral ratio between surface and bedrock at the node C2.

The permanent deformation along the SW-NE section and the time histories of the horizontal and vertical displacements of three surface points on the calcarenitic plateau are shown in Figure 12. A horizontal final displacement of about 79cm resulted at point C2a towards the SW direction; instead, a much lower displacement (about 18cm) is computed at the opposite ridge point C2b in NE direction (Fig. 12c). The distribution of vertical permanent displacements at the same points (Fig. 12c) is also strongly non-uniform, with a differential settlement of about 30-35 cm between the SW slope and the central-NE part of the slab.

In addition, the final deformation pattern, using Landers earthquake, along the transversal section of the hill is shown in terms of contours referred to the horizontal displacements (Fig. 12a) and vectors of the total displacements (Fig. 12b). Both plots confirm that a rigid rotational sliding of the SW side of the calcarenite slab occurs above the sand layer. The graphs also show displacements as high as about 1m in the varicoloured clay, close to the contact with the conglomerates; the overall distribution seems to highlight the triggering of a mainly translational mechanism of slope instability at the toe of the hill, due to the increment of inertia forces in the shallowest layers induced by swelling, as already evidenced in Fig. 9.

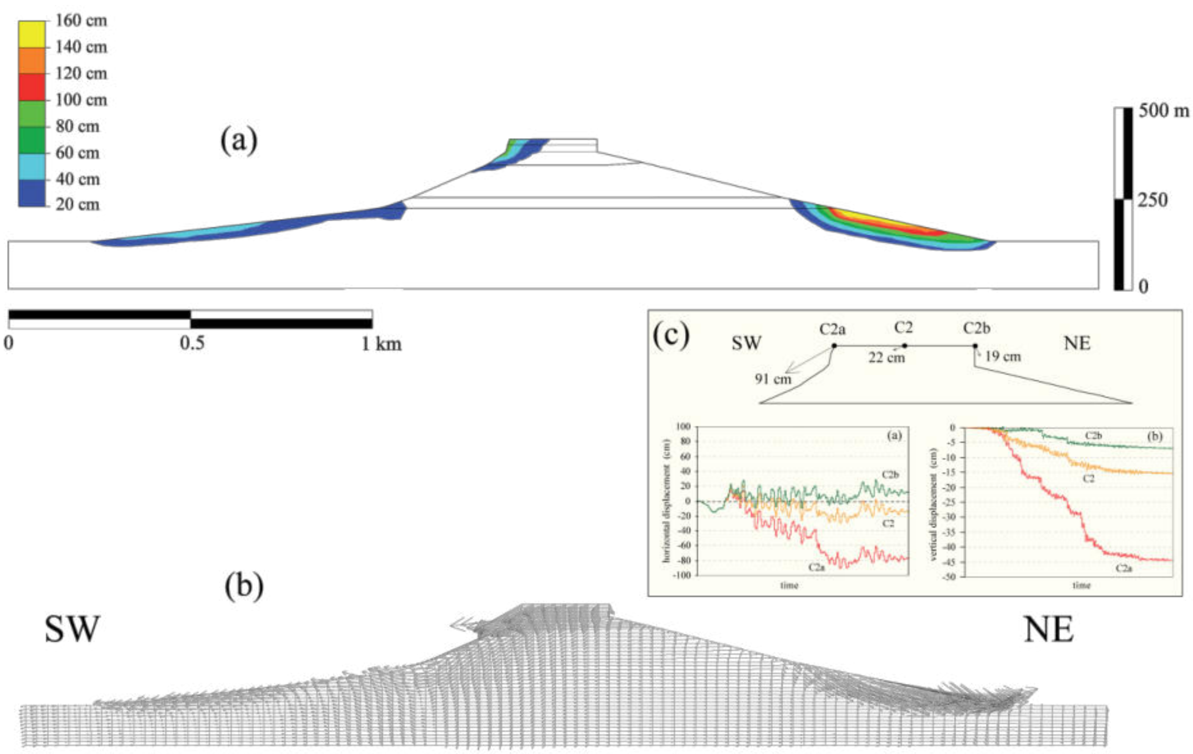

Figure 12. Distribution of permanent displacements, using Landers earthquake, along the section SW-NE: contour of the horizontal component (a) and total vectors (b). Time histories of the horizontal and vertical displacements of three surface points on the calcarenitic plateau (c).

The same behaviour of the cliff is obtained using the other input motions, however the maximum horizontal displacements at the end of the simulation are strongly dependent on the selected earthquake. In fact, the results show maximum permanent displacements between some tens of centimeters, for Loma Prieta and Northridge, and hundreds of centimeters, for Landers and Imperial Valley. These differences are probably related to the higher energy contents in correspondence of the period range of maximum amplification (i.e., periods between 1s and 2s as shown in Fig. 11c), and also to the longer durations of the acceleration time histories recorded during the Landers and Imperial Valley earthquakes.

7. CONCLUSIONS

The study aims to contribute to the understanding of the seismic behaviour of the Gerace cliff - a fragile site particularly exposed to the environmental risks -, that is characterized by a peculiar geological arrangement and hosts an invaluable historical and architectural heritage. Since the chronicles report significant environmental effects, as well as to relevant damaging of the built, around the inhabited area of Gerace in the occurrence of historic earthquakes (although with epicenters at several tens of kilometers away), the authors decided to addressed the analysis of the seismic response of the hill. Not to forget the past, but rather to learn from it. The research activity consisted in examining the different elements necessary to an overall assessment, supporting the definition of the reference seismic scenario, the study of the geological setting, the geotechnical characterization of the soils and the numerical modelling. Thus, the findings also allowed to learn some useful lessons which can result of more general interest and application for the seismic safety of comparable historical towns and other strategic sites.

A seismic hazard analysis was used for the simulation of the seismic response of the cliff to the maximum historical earthquake, allowing to back-figure the input motions representative of the first earthquake of the anomalous sequence occurred in Southern Calabria in 1783. It is worth noting that this highly hazardous area can be realistically subjected to fault interaction mechanisms (Peruzza et al., 1997).

An accurate geotechnical characterisation was based on previous investigations available and on specifically arranged field and laboratory tests on the different soils and soft rocks characterising the hill. The test results highlighted that most of the materials have rather peculiar behaviour, nevertheless suggesting that more comprehensive experimental studies would better integrate the mechanical properties used for the dynamic analyses. A more detailed description of the subsoil model in both longitudinal and transversal directions of the hill might be available after appropriate deep geophysical investigations. For instance, the residual unknowns on the bedrock nature, depth and geometry should be better investigated by electric resistivity tomographies and/or seismic refraction tests.

The results of 1D and 2D numerical simulations evidenced the distinct effects of both stratigraphy and topography on the variability of ground motion amplification through the town centre and along the slopes. The computed permanent strains and displacements could justify the occurrence of accumulated large deformations following the seismic sequence, reported by the chronicles. In particular, the overall deformation pattern seems to indicate that the fracturing processes of the plateau induced by the erosion might have been intensified in occurrence of these historical earthquakes. In fact, plastic strains develop throughout the sands layer, indicating a tendency to slippage of the calcarenite layer along the contact with the underlying sand. In addition, the increment of the inertial forces may have contributed both to the sliding of calcarenitic blocks at the borders of the slab and the slope instability at the base of the relief.

However, a better understanding of deep geomorphological factors and groundwater conditions, might address more reliable evaluations of the interplay between hydrogeological and seismic hazard on the environmental risk of such a precious heritage. Such predictions would more consciously support the design of consequent mitigation countermeasures.

ACKNOWLEDGMENTS

Some parts of this study was performed in the framework of the *S3 Research Project 2004-06*, promoted by *Istituto Nazionale di Geofisica e Vulcanologia* (INGV) and funded by the *Dipartimento di Protezione Civile* (DPC) of the Italian Government. Therefore, the authors are indebted to the DPC and to the project team coordinators, Dr. Francesca Pacor and Prof. M. Mucciarelli, for their valuable support. Profs. J.P. Stewart, G. Lanzo, F. Bozzano, S. Martino and I. Guerra, as well as Dr. F. Galadini and Dr. P. Tommasi are also warmly acknowledged for the fruitful discussions and suggestions. The authors are also grateful to the anonymous reviewers and the Editor-in-Chief Prof. L. N.Y. Wong for their constructive comments which helped us improve the quality of the manuscript.

REFERENCES

1. Ambraseys N.N. (1995) The prediction of earthquake peak ground acceleration in Europe, Earthquake Engineering and Structural Dynamics, 24(4):467–490.
2. Bardet J. P., Ichii K. and Lin C.H. (2000) A computer program for Equivalent-linear Earthquake site Response Analyses of layered soil deposits (EERA), University of Southern California, Department of Civil Engineering.
3. Bommer J. J. and Acevedo A. B. (2004) The use of real earthquake accelerograms as input to dynamic analysis, Journal of Earthquake Engineering, 8(1):43-91.
4. Boschi E., Guidoboni E., Ferrari G., Mariotti D., Valensise G. and Gasperini P. (2000) Catalogo dei Forti Terremoti in Italia dal 461 a.C. al 1997 d.C., Istituto Nazionale di Geofisica, Storia Geofisica Ambiente
5. Bray J.D. and Travarasau T. (2007) Simplified procedure for estimating earthquake-iInduced deviatoric slope displacements, Journal of Geotechnical and Geoenvironmental Engineering, 133(4):381-392. DOI: 10.1061/(ASCE)1090-0241(2007)133:4(381)
6. Carbone Grio D. (1884) Terremoti di Calabria e Sicilia nel secolo XVIII, Napoli, G. de Angelis e figlio tipografi.

7.Costanzo A. (2007) Analisi di fenomeni deformativi di pendii e rilievi in condizioni sismiche: il caso di Gerace, Ph.D. thesis, University of Calabria.

8.Costanzo A, d'Onofrio A, Lanzo G, Pagliaroli A, Penna A, Puglia R, Santucci De Magistris F, Sica S, F. Silvestri, Tommasi P (2007a). Seismic response of historical centers in Italy: selected case studies. In: Pitilakis. Workshop on 'Geotechnical Earthquake Engineering related to Monuments and Historical Centers'. Thessaloniki, Greece, 2007, p. 1-24, Dordrecht: Springer, ISBN:9781402058936.

9.Costanzo A., d'Onofrio A., Silvestri F. (2007b). Numerical simulations of the ground deformation recorded in the historical town of Gerace during the seismic events in Calabria (1783). In: k. Pitilakis. Earthquake geotechnical engineering. Thessaloniki, 25-28 giugno 2007, p. 1-8, Dordrecht: Springer, ISBN: 9781402058929

10. Cotecchia V., Guerricchio A. and Melidoro G. (1986) The geomorphogenetic crisis triggered by the 1783 earthquake in Calabria (Southern Italy), Proceedings of the Symposium on Engineering Geology Problems in Seismic Areas, Bari, 6:245-304, International Associati.on of Engineering Geology

11. d’Onofrio A., Olivares L. and Santucci de Magistris F. (1998) Influence of soil structure on the behaviour of two stiff Italian clays in the pre-failure range, Proceedings of the II International Symposium on the Geotechnics of Hard Soils and Soft Rocks, Napoli, 1:497-506. Rotterdam: Balkema.
12. d’Onofrio A., Silvestri F. and Vinale F. (1999) A new torsional shear device, ASTM Geotechnical Testing Journal, 22(2):107-117.
13. DISS Working Group (2018). Database of Individual Seismogenic Sources (DISS), Version 3.2.1: A compilation of potential sources for earthquakes larger than M 5.5 in Italy and surrounding areas. http://diss.rm.ingv.it/diss/, Istituto Nazionale di Geofisica e Vulcanologia; DOI:10.6092/INGV.IT-DISS3.2.1.
14. Evangelista L., Landolfi L., d'Onofrio A, Silvestri F. (2016) The influence of the 3D morphology and cavity network on the seismic response of Castelnuovo hill to the 2009 Abruzzo earthquake. Bulletin of Earthquake Engineering 14 (12), 3363-3387
15. Faccioli E, Vanini M, Frassine L (2002) “Complex” site effects in earthquake ground motion, including topography. Proceedings of the 12th European conference on earthquake engineering, n.884, 9-13th September 2002, London, UK.
16. Fenelli G.B., Picarelli L., Silvestri F. (1992) Deformation process of a hill shaken by the Irpinia earthquake in 1980, Proceedings of the French-Italian Conference on "Slope stability in seismic areas", Bordighera (Italy), 47-62, Ouest Editions Presses Académiques
17. Fenelli G.B., Pellegrino A. and Picarelli L. (1998) Stability problems of old towns built o relict plateaux on clay deposits, Proceedings of the International Symposium on Geotechnical Engineering for the Preservation of Monuments and Historic Sites, Napoli, 163-173. Rotterdam: Balkema.
18. Fortunato C., Martino S., Prestininzi A., Romeo R.W., coauthors Fantini A., Sanandrea P. (2012). New release of the Italian catalogue of earthquake-induced ground failures (CEDIT). Italian Journal of Engineering Geology and Environment, DOI: 10.4408/IJEGE.2012-02.O-05
19. Galli P. and Bosi V. (2002) Paleoseismology along the Cittanova fault: implications for seismotectonics and earthquake recurrence in Calabria (Southern Italy)”, Journal of Geophysical Research, 107(B3) 2044, ETG 1:1-19.

20. Guerricchio A. (2005) Tectonics, Deep Seated Gravitational Slope Deformations (DSGSDs) and Large Landslides in the Calabrian Region (Southern Italy), Giornale di Geologia Applicata, 1: 73-90, DOI: 10.1474/GGA.2005-01.0-08.0008
21. Hardin B.O. and Drnevich V.P. (1972) Shear modulus and damping in soils: design equations and curves, Journal of the Soil Mechanics and Foundations Division, ASCE, 98(SM7):667-692.
22. Hashash Y.M.A. and Park D. (2002) Viscous damping formulation and high frequency motion propagation in non-linear site response analysis, Soil Dynamics and Earthquake Engineering, 22:611-624.
23. Huang Y., Xiong, M., Zhou H. (2015) Ground seismic response analysis based on the probability density evolution method, Engineering Geology, 198: 30-39, DOI: 10.1016/j.enggeo.2015.09.004
24. Itasca Consulting Group (2005) Flac 5.0 USER'S Manual, Minneapolis, Minnesota, USA.
25. Joyner W.B. and Boore D.M. (1981) Peak horizontal acceleration and velocity from strong-motion records including the records from the 1979 Imperial Valley, California, earthquake, Bulletin of the Seismological Society of America, 71:2011-2038.
26. Kuhlemeyer R.L. and Lysmer J. (1973) Finite element method accuracy for wave propagation problems, Journal of the Soil Mechanics and Foundations Division, ASCE, 99(SM5):421-427.
27. Lampitiello S., Olivares L., Silvestri F. (2001) Numerical simulation of seismic and post-seismic response of Bisaccia hill, TC4 Earthquake Geotechnical Engineering Satellite Conference on 'Lessons learned from recent strong earthquakes', XV ICSMGE, Istanbul, Turkey.
28. Landolfi L., Evangelista L., Chiaradonna A., d'Onofrio A., Silvestri F. (2014) Analisi della risposta sismica locale del colle di Castelnuovo - Proceedings of the XXV Convegno Italiano di Geotecnica. Baveno 4-6 giugno 2014, 2:177 - 184.
29. Lanzo G., Olivares L., Silvestri F., Tommasi P. (2004) Seismic response analysis of historical towns rising on rock slabs overlying a clayey substratum, Proceedings of the V International Conference on 'Case Histories in Geotechnical Engineering, Paper No. 3.25, New York, USA.

30. Lanzo G., Silvestri F., Costanzo A., D'Onofrio A., Martelli L., Pagliaroli A., Sica S., Simonelli A. (2011) Site response studies and seismic microzoning in the Middle Aterno Valley (L'Aquila, Central Italy)", Bulletin of Earthquake Engineering, 9(5):1417-1442.
31. Lo Presti D.C.F., Jamiolkowski M., Pallara O., Cavallaro A. and Pedroni S. (1997) Shear modulus and damping of soils, Geotechnique, 47(3): 603-618.
32. Lysmer J. and Kuklemeyer L. (1969) Finite dynamic model for infinite media, Journal of the Engineering Mechanics Division, 859-877.
33. Massa, M., Barani, S., Lovati, S. (2014) Overview of topographic effects based on experimental observations: meaning, causes and possible interpretations. Geophysical Journal International, 197(3): 1537–1550, https://doi.org/10.1093/gji/ggt341
34. Marcellini A., Iannaccone G., Romeo R.W., Silvestri F., Bard P.Y., Improta L., Meneroud J.P., Mouroux P., Mancuso C., Rippa F., Simonelli A.L., Soddu P., Tento A., and Vinale F. (1995), The Benevento Seismic Risk Project: I - Seismotectonic and geotechnical background, Proceedings of the V International Conference on Seismic Zonation, Nice. Nantes: Ouest Editions Presses Académiques.
35. Meletti C., Valensise G., Azzaro R., Barba S., Basili R., Galadini F., Gasperini P., Stucchi M. and Vannucci G. (2004) Zonazione Sismogenetica ZS9. App.2 al Rapporto Conclusivo. – Gruppo di lavoro della mappa di pericolosità sismica (PCM n.3274/03), Istituto Nazionale di Geofisica e Vulcanologia (INGV), Rome, Italy.
36. Monteleone S. (1993) Deformazioni gravitative profonde e grandi frane indotte dalle argille varicolori scagliose a Gerace e liquefazione nei terreni del territorio di Locri, M.Sc. thesis, University of Calabria.
37. Olivares L. and Silvestri F. (2010) A laboratory and numerical investigation on a post-seismic induced settlement in Southern Italy, Proceedings of the IV International Conference on 'Recent Advances in Geotechnical Earthquake Engineering and Soil Dynamics', Paper No. 10.30, S. Diego, USA.
38. Pagliaroli A., Lanzo G., D'Elia B. (2011) Numerical evaluation of topographic effects at Nicastro ridge in southern Italy, Journal of Earthquake Engineering , 15(3): 404-432.
39. Pagliaroli A. and Lanzo G. (2008) Selection of real accelerograms for the seismic response analysis of the historical town of Nicastro (Southern Italy) during the March 1638 Calabria earthquake, Engineering Structures, 30(9): 2211-2222.

40. Paolucci R. (2002) Amplification of earthquake ground motion by steep topographic irregularities, Earthquake Engineering and Structural Dynamics, 31: 1831-1853.
41. Peruzza L., Pantosti D., Slejko D. and Valensise G. (1997) Testing a new hybrid approach to seismic hazard assessment: an application to the Calabrian Arc (Southern Italy), Natural Hazards 14: 113-126.
42. Pitilakis K, (2004) "Chapter 5: Site Effects", in: Recent advances in Earthquake Geothecnical Engineering and Microzonation, Atilla Ansal ed., Kluwer Academic Publishers, pp. 139-198.
43. Rampello S., Silvestri F. and Viggiani G. (1994) The dependence of small strain stiffness on stress state and history for fine-grained soils: the example of Vallericca clay, Proceedings of the I Symposium on Pre-failure Deformations of Geomaterials, Sapporo, 1:273-279. Rotterdam: Balkema.
44. Rovida A., Locati M., Camassi R., Lolli B., Gasperini P. (eds.), 2016. Catalogo Parametrico dei Terremoti Italiani, versione CPTI15. Istituto Nazionale di Geofisica e Vulcanologia. DOI: http://doi.org/10.6092/INGV.IT-CPTI15
45. Sabetta F. and Pugliese A. (1987) Attenuation of peak horizontal acceleration and velocity from Italian strong motion records, Bulletin of the Seismological Society of America, 77(5):1491–1513.
46. Sabetta F. and Pugliese A. (1996) Estimation of response spectra and simulation of nonstationary earthquake ground motions, Bulletin of the Seismological Society of America, 86 (2): 337-352.
47. Sanchez-Sesma F. J. (1990) Elementary solutions for response of a wedge-shaped medium to incident SH and SV waves, Bulletin of the Seismological Society of America, 80(3): 737-742.
48. Sica S, Russo AD, Rotili F, Simonelli AL (2014) Ground motion amplification due to shallow cavities in nonlinear soils. Natural hazards 71 (3), 1913-1935.
49. Vucetic, M. (1994) Cyclic threshold shear strains in soils, Journal of Geotechnical Engineering, ASCE, 120(12):2208-2228.
50. Wells D.L. and Coppersmith K. J. (1994) New empirical relationships among magnitude, rupture length, rupture width, rupture area, and surface displacement, Bulletin of the Seismological Society of America, 84:974-1002.